ROYAL SOCIETY
OF CHEMISTRY

REVIEW ARTICLE
Liguang Wang, Shun Wang, Huile Jin *et al.*
Challenges of layer-structured cathodes for sodium-ion batteries

NCNST

REVIEW

Check for updates

Challenges of layer-structured cathodes for sodium-ion batteries

Caihong Shi,[a] Liguang Wang, [ID] *[ab] Xi'an Chen, [ID] [a] Jun Li,[a] Shun Wang, [ID] *[a] Jichang Wang[b] and Huile Jin [ID] *[a]

As the most promising alternative to lithium-ion batteries (LIBs), sodium-ion batteries (SIBs) still face many issues that hinder their large-scale commercialization. Layered transition metal oxide cathodes have attracted widespread attention owing to their large specific capacity, high ionic conductivity, and feasible preparation conditions. However, their electrochemical properties are usually limited by the irreversible phase transition and harsh storage conditions caused by humidity sensitivity. Recently, tremendous efforts have been devoted to solving these issues toward advanced high-performance layered oxide cathodes. Herein, we summarize these remaining challenges of layered oxide cathodes and the corresponding modification strategies such as the variations in chemical compositions, the architecture of (nano)micro-structures, surface engineering, and the regulation of phase compositions. We hope that the understanding presented in this review can provide useful guidance to developing high-performance layer-structured cathode materials for advanced SIBs.

1. Introduction

With the continuous consumption of non-renewable energy and the intensification of environmental pollution problems, clean and renewable energy has received widespread attention. As an efficient and clean energy source, rechargeable secondary batteries can effectively alleviate the current energy and environmental problems.[1,2] Lithium-ion batteries (LIBs) have been developed and commercialized by Sony in 1991. Due to their advantages of high energy density, long service life, low self-discharge rate, low maintenance cost, and good safety, LIBs are widely used in portable electronic products. Although the LIB technology is mature, LIBs still have problems in terms of safety, longevity, poor low-temperature performance, and high cost.[3–8] In addition, with the widespread use of electric vehicles and portable electronic devices, the increasing demand for lithium, coupled with the limited reserves of lithium ore, is further pushing up the price of LIBs. Therefore, the search for lower cost batteries has attracted increasing attention. The sodium element in the same main group as lithium has been tremendously studied by virtue of its abundant reserves in nature.[9] However, the energy density and cycle stability of sodium-ion batteries (SIBs) are still far from satisfying the need

for electric vehicles and energy storage systems, owing to the relatively low working voltages compared to lithium systems. A key issue for SIBs to meet the growing requirements of electronic products is to find cathode materials with high energy density and excellent cycle performance.[10–14]

Cathode materials for SIBs mainly include polyanion-type compounds, Prussian blue compounds, tunnel-type oxides, layered transition metal oxides, *etc.*[15] The polyanion-type compound has a strong covalent bond between the transition metal and oxygen polyhedron (MO_x), which can form a structure composed of two-dimensional van der Waals bonding or a three-dimensional framework, leading to fast alkali ion migration pathways. The diversity and stability of the structure, coupled with the strong induction effect of polyanionic compounds, result in a suitable working voltage and excellent electrochemical properties. However, the complicated synthesis and poor electric conductivity hinder their further large-scale applications.[16] The transition metal ions in Prussian blue compounds are connected by CN coordination to form a three-dimensional cubic network structure. This allows Na^+ to have a large transfer channel, leading to a large diffusion coefficient, and excellent rate performance. However, these compounds usually contain crystal water that is difficult to control upon material preparation, resulting in a low tap density that affects the energy density of the battery system.[17–20] Tunnel-type oxides have good structural stability, but show a low theoretical capacity due to the small sodium content (less than one).[21,22] The layered transition metal oxide Na_xTMO_2 ($0 < x \leq 1$, TM = Fe, Ni, Co, Mn, *etc.*) has become the

[a] *Key Laboratory of Leather of Zhejiang Province, Institute of New Materials and Industrial Technologies, Wenzhou University, Wenzhou, China.*
E-mail: huilejin@wzu.edu.cn, shunwang@wzu.edu.cn
[b] *Department of Chemistry and Biochemistry, University of Windsor, Windsor, ON, Canada. E-mail: lgwang.hit@gmail.com*

most promising cathode material for SIBs owing to its large specific capacity, high ionic conductivity, and feasible preparation conditions. However, these materials still have some critical issues, such as instability in humid air, which severely limit their further commercialization.[10,11,18,23,24] One of our efforts to solve these problems is through understanding and subsequently reducing the gap between the theoretical and actual capacities, so that the electrode can more efficiently release its capacity potential during the long cycle.

This review uniquely summarizes the latest progress in current layered transition metal oxide electrodes by pointing out the problems faced by such materials in the cycling process and discussing the widely used modification strategies for overcoming these problems. To understand the properties of the material, one needs to understand its structure first. The way that oxygen atoms accumulate in different phases of the material is different, which leads to different interlayer distances and coordination environments for cations, *etc.* The main challenges that are faced by Na_xTMO_2 materials are the severe irreversible phase transitions when cycling at a high cutoff voltage, storage instability caused by environmental sensitivity, and poor electrochemical performance induced by the above-mentioned issues. The current solutions to these problems are also comprehensively summarized from the following four aspects, *i.e.*, variations in chemical compositions, the architecture of nano-micro structures, surface engineering, and the regulation of phase composition. Existing studies have shown that the selection and design of a synthesis method influence the performance of the prepared materials. On this front, this review makes a brief comparison of the advantages and disadvantages of several representative synthesis methods, hoping to provide meaningful guidance for the development of new electrode materials with high energy density and long cycle life (Fig. 1).

2. Crystal structure of layered oxides

Layered transition metal oxides (Na_xTMO_2) can generally be divided into two configurations according to the different coordinations of Na^+ of P-type and O-type including P2, P3,

O2, and O3 types based on the atomic arrangement (Fig. 2a–d).[25] O and P indicate the position of Na^+ in the structure, where P indicates that Na^+ occupies the triangular prism site between the TMO_6 interlayers, O indicates that Na^+ is located on the octahedral site between the TMO_2 layers, and the number denotes the number of transition metal layers in the structural unit. Specifically, the O3-type structure can be classified into 3R phase, $R\bar{3}m$ space group, which is also the common structure similar to $LiCoO_2$. The stacking method is ABCABC, with three different TMO_2 layers AB, AC, and BC, and all the Na^+ are located on the same octahedral site of the $Na–O_6$ coordination. The O3 structure oxide usually has high sodium content close to full occupation on the sodium site. For the O3-type structure, the diffusion of sodium from one octahedral position to another octahedral position occurs through the interstitial tetrahedral position shared by the faces, and the diffusion speed is relatively slow.[10] The P2 type belongs to the 2H phase that corresponds to the $P6_3/mmc$ space group, and there are two TMO_2 layers: AB and BA. There are two different sites for Na^+ in this structure. The shared edge with the TMO_6-octahedron in two adjacent plates is marked as Na_e (1/3 2/3 1/4), and the shared surface is marked as Na_f (0 0 1/4). But Na^+ cannot exist at the two sites at the same time, because the radius of Na^+ is about 2.04 Å, which is much larger than the distance between Na_e and Na_f (≈ 1.67 Å). Generally speaking, there is an open channel for Na^+ in the P2-type structure, which can enhance the diffusion of Na^+ and provide high capacity. However, the initial Na content of the P2 electrode is usually lower than that of the O3 electrode, which limits the storage capacity at the first charge.[26] The P3-type structure, as a thermodynamically metastable phase, is generally synthesized at a lower temperature and generally has a higher initial
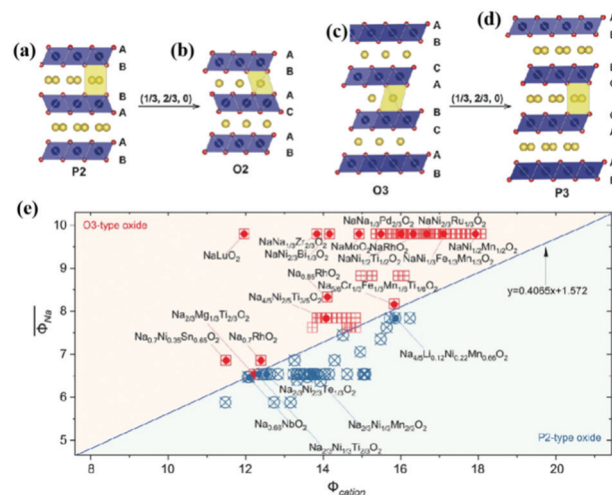

Fig. 1 Main challenges and solutions of SIB layered cathode materials.

Fig. 2 Schematic diagram of the crystal structure of layered Na_xTMO_2 oxides for (a) P2 type, (b) O2 type, (c) O3 type and (d) P3 type. The blue and yellow spheres represent transition metals and Na^+, respectively. Adapted with permission.[10] Copyright 2017, Wiley-VCH. (e) Cation potential of representative P2 and O3 sodium ion layered oxides. Adapted with permission.[33] Copyright 2020, American Association for the Advancement of Science.

capacity but poorer cycling performance. Since its layer spacing is larger than that of the P2 phase, it provides a wider path for the diffusion of Na^+, so it generally exhibits better multiplicative performance. Because of this, P3-type cathode materials are more likely to absorb water from the environment, leading to the exchange of Na^+ with H^+, which to some extent limits the application of P3-type materials. At present, there are relatively few research reports on this type of material, and more materials and properties need to be further investigated.[27–29] The O2 phase material belongs to the oxygen stacking mode of ABAC. This phase is usually produced by the detachment of Na^+ and the reduction of interlayer distance during the charging and discharging process of the P2 phase material. Such an irreversible phase change will lead to the deterioration of cycling performance. Overall, P2 and O3 represent the most studied phases. In addition to the previously mentioned single-phase materials, multi-phase composites are gradually attracting more and more attention. Biphasic synergistic effects have been reported for laminated P2/P3 and P2/O3 composites. By uniting the multiphases, the advantages of each phase are exploited, resulting in the thus-achieved cathodes with high electrochemical performance.[30–32]

Composition determines the structure of a material, which subsequently affects its properties. Therefore, if one can predict the structure of a material from its composition, this will then provide a useful guide for the design of optimal layered oxide materials. The phases in layered oxides can be determined by the optimization of chemical compositions based on various transition metal redox. The electron distribution plays a very important role in the competition between the P-type and O-type layered oxides, which significantly affects their working potentials. Zhao et al.[33] introduced the cation potential $\Phi_{cation} = \dfrac{\overline{\Phi_{TM}}\,\overline{\Phi_{Na}}}{\overline{\Phi_O}}$ to express the electron density and polarization of the cation. They designed a specific superimposed structure by controlling the sodium content and transition metal composition of the synthetic material. The reported phase diagram of the Φ_{cation} and $\overline{\Phi_{Na}}$ of the P2 and O3 materials (Fig. 2e) shows that the Φ_{cation} can accurately describe the competition between the P2 and O3 structures of the layered structure material. Generally, the larger the cation potential, the stronger the interlayer repulsion and the expansion of the transition metal electron cloud, which tends to favor the P2-type structure and increase the d(O–Na–O). On the contrary, one can increase the content of Na to obtain a higher $\overline{\Phi_{Na}}$, which can enhance the shielding effect of electrostatic repulsion between the TMO_2 plates and make it more prone to form O3 type. However, this is only an empirical prediction method, which may not provide robust theoretical guidance for entropy-dominated phases, metastable phases and disordered compounds that should be based on the actual synthesized materials.

3. Preparation of layer-structured oxides

The selection and design of a synthesis method are critical for achieving specific crystal structures that can be used in high-performance SIBs. Various synthesis methods yield great differences in structure, particle size, morphology, and electrochemical properties. Therefore, one can optimize the synthesis procedure to achieve the desired morphology, particle size, crystallinity, and phase purity of the materials. The most commonly used synthesis method is the solid-state method, which is mainly due to its simple preparation process and easy operation.[34–38] For example, Wang et al.[35] used $NaCH_3COOH$ as the sodium source, mixed it with a certain stoichiometric ratio of K_2CO_3 and MnO_2, ball milled for 12 hours, and added a small amount of acetone as a dispersant to make the materials uniformly mixed. The dried powder is calcined at a high temperature to obtain the $P2–Na_{0.67-x}K_xMnO_2$ material. Yao et al.[39] synthesized the Cu/Ti co-doped $O3–Ni_{0.45}Cu_{0.05}Mn_{0.4}Ti_{0.1}O_2$ material via a solid-state method. Wang et al.[40] also used this method to study the effect of Mg doping on the $Na_{0.7}[Mn_{0.6}Ni_{0.4}]O_2$ material. Obviously, the high-temperature solid-state method provides great convenience for studying the effects of element doping types and doping amounts on the electrochemical properties of materials. The selection of precursors and calcination conditions in the solid-state method will have a great impact on the materials, especially the calcination temperature. In the phase diagram of the Na_xCoO_2 material, it can be found that the sodium content and synthesis temperature have a great impact on the phase of the material.[41] At a low sodium content ($0.6 < x < 0.75$), the P2 phase is more likely to form at high temperatures, and O3 phase is easy to form at a high sodium content. However, in addition to the thermodynamically stable P2 and O3 phases, thermodynamically metastable phases P3 and O3′ may also be formed, which is the result of the complex interaction of thermodynamics and kinetics in the process of material synthesis. At the same time, it provides some guidance for the selection of precursor and synthesis temperature in material synthesis. The essence of a solid-phase method is ion diffusion. The materials synthesized by this method cannot completely reach the uniformity of the atomic level, and the morphology and particle size are difficult to control. Therefore, the solution method is used to prepare cathodes with controllable morphology and fine particle size.

Co-precipitation is a common method that is widely applied in industries.[42–46] Generally, the preparation of cathode materials is divided into two steps. First, using an appropriate precipitant, and adjusting pH, one can precipitate the evenly mixed metal ions in the solution. Upon filtration, washing and then drying to obtain the precursor, the precipitates are then mixed with sodium salt and calcined to obtain the target product. Sun et al.[47] synthesized the nanorod gradient $Na[Ni_{0.65}Co_{0.08}Mn_{0.27}]O_2$ cathode via co-precipitation. The material is composed of a high-capacity Ni-rich core and Mn-rich surface with high cycle stability. In the synthesis process, Ni/Co/Mn ionic solutions with different molar ratios are pumped into the reactor in order to control the change of the chemical composition gradient of the material from inside to outside. The concentration, temperature, pH and stirring speed of the solution should be accurately controlled in order to obtain spherical particles with uniform size distribution and

are composed of small needle-like primary particles. The reaction is carried out in solution, the reactants can be fully mixed, the size and morphology of the prepared materials are more controllable, and the uniformity is much higher than that of the solid-state method. However, the reaction temperature, pH of the solution and stirring speed need to be accurately controlled in the synthesis process, resulting in a relatively high synthesis cost.

The sol–gel method is also a good choice for reducing the production cost and obtaining uniform high-performance materials.[31,32,48–50] The sol–gel method is used to adjust the pH and temperature of the solution, so that the transition metal salt ions react with the complexing agent in the solution, thus forming transparent sol. After dehydration and drying, the gel is obtained and calcined to obtain the oxide. Yang et al.[31] synthesized the $Na_{0.8}Li_{0.2}Fe_{0.2}Mn_{0.6}O_2$ material with the P2/O3 biphase with metal nitrate as the raw material and citric acid as the chelating agent. The initial reversible capacity of the material was 174 mA h g^{-1}. The precursor materials prepared by this method are evenly mixed and have a low production cost, but the reaction time is too long and is not easy to industrialize production.

In addition, many other methods have been used to prepare high-performance Na_xTMO_2 materials. The combustion method is a relatively simple one, which can use the heat released by itself to maintain the reaction, so it can be used as a low-cost synthesis method.[51–54] Aishuak Konarov et al.[53] dissolved nitrate in water, used citric acid as the fuel, heated the solution at 100 °C to evaporate the aqueous solution, then increased the temperature to 200 °C and the material started to show spontaneous combustion. After that, they heated the material to 500 °C to remove nitrate and carbon residues in the material, and calcined at 900 °C to obtain the final material. Although the combustion synthesis process is very fast, the controllability of the combustion process and the morphology are poor. In fact, spray drying is effective to disperse the materials to be dried through an atomizer and disperse them into atomized droplets.[55] When exchanged with hot air, it evaporates moisture and gives dry powder materials. The drying speed is relatively fast, and the operation control is convenient and suitable for large-scale production, but the requirements for a spray dryer are high. In addition, Na_xTMO_2 materials have also been synthesized by solvothermal method,[56] thermal

polymerization[57,58] and modified Pechini.[59] Each method has its own relative merits, has different requirements for production environment and cost, and has different effects on the size, morphology and purity of materials. Table 1 provides a brief comparison of the advantages and disadvantages of several frequently deployed synthesis methods. Therefore, in order to develop better layered transition metal materials, the preparation process needs to be continuously optimized.

4. Challenges of layer-structured oxides

There are three main challenges, i.e., irreversible phase transitions, structural instability caused by humidity sensitivity and electrochemical degradations, which hinder the application of layered oxides. Through in situ XRD, one can observe that a P2–O2 phase transition usually occurs in P2-type materials, and O3-type undergoes a more complex phase transition. The occurrence of this irreversible phase transition will lead to structural degradation and capacity decay of the cathode material. Moreover, the laminate materials are very sensitive to the environment, where moisture and CO_2 in the air will affect the materials to some extent. Meanwhile, side reactions with the electrolyte will lead to the degradation of the electrochemical properties of the materials. Herein, in this section, we summarize the main issues in the layer-structured materials with these aspects.

4.1 Irreversible phase transitions

In general, the P2 and O3 phases undergo a series of phase transitions during the electrochemical cycle, involving different stacking sequences of the oxygen layer.[60] During the charging and discharging process, the P2 phase usually transits to the O2 phase due to the sliding of TMO_6 octahedral layers with the extraction of Na$^+$. These problems result in a significant shrinkage of the crystal structure and a reduction in the distance between layers. Conversely, in the O3 phase, Na initially stabilizes at the TMO_6 octahedral position shared by the edges. When the sodium ions are partially extracted from the O3 phase, the Na in the center of the prism becomes energy stable, which is related to the formation of vacancies, similar to the P2 phase. Then, a wide prism center is formed by sliding the

Table 1 Advantages and disadvantages of different synthetic methods for the preparation of sodium ion layered transition metal oxides

| Synthetic method	Advantages and disadvantages	
	Advantages	Disadvantages
Solid-state method	Simple preparation process, easy operation	Poor uniformity of materials; morphology and particle size are difficult to control
Co-precipitation	The size and morphology are more controllable, the uniformity is much higher	Strict synthesis conditions, high synthesis cost
Sol–gel method	Low production cost, high uniformity	Reaction time is too long, not easy to industrialize
Combustion method	Low-cost, fast synthesis process	Poor control of combustion process and morphology
Spray drying	Fast drying speed, convenient operation and control, suitable for large-scale production	The requirements for spray dryer are high
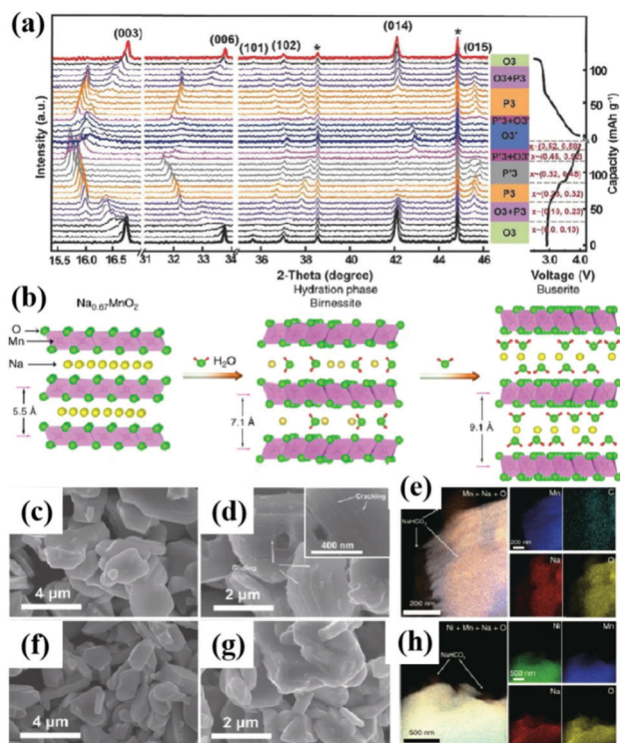
Fig. 3 (a) *In situ* XRD pattern of $NaFe_{0.45}Co_{0.5}Mg_{0.05}O_2$ (NaFCM) during the first cycle of charging and discharging at 2.0–4.5 V; adapted with permission.[61] Copyright 2017, Wiley-VCH. (b) Influence of water absorption on the structure of the $P2–Na_{0.67}MnO_2$ material;[38] the SEM images of (c) pristine and (d) relative humidity (RH) 93% + CO_2 exposed $Na_{0.67}MnO_2$ powder, (e) the EDS mapping results of exposed $Na_{0.67}MnO_2$, indicating that $NaHCO_3$ is formed on the particles' surface. SEM images of (f) pristine and (g) RH 93% + CO_2 exposed $Na_{0.67}Ni_{0.33}Mn_{0.67}O_2$ powder, (h) the EDS mapping results of RH 93% + CO_2 exposed $Na_{0.67}Ni_{0.33}Mn_{0.67}O_2$ samples, $NaHCO_3$ particles are also observed on the surface of exposed $Na_{0.67}Ni_{0.33}Mn_{0.67}O_2$. Adapted with permission.[38] Copyright 2020, All Rights Reserved.

TMO_2 sheet without breaking the TM–O bond. Therefore, the typical oxygen accumulation changes from "ABCABC" to "ABBCCA", which is classified as a P3 phase. For $NaNi_{0.5}Mn_{0.5}O_2$, the O3 phase often undergoes a more complex phase transition (Fig. 3a) than the P2 structure,[61,62] such as O3 → O′3 → P3 → P3″, while the P2 phase usually exhibits a P2–O2 phase transition which can be observed by *in situ* XRD.[63–67] Therefore, due to its good structural integrity and low diffusion barrier, P2 structured oxides always show good cycle stability and rate capability.[68]

4.2 Structural instability caused by humidity sensitivity

The hygroscopic properties of layered cathode materials after exposure to air result in poor battery performance and increased transportation costs. The layered structure oxides are very sensitive to the moisture environment. For example, in a humid environment, water molecules will enter the sodium layer, leading to dramatic structural evolution. CO_2 will also have a certain impact on these materials, which can form electrochemically inactive NaOH and Na_2CO_3 when reacted with the oxides.[26] So far, there is still a lack of in-depth and

systematic understanding of the reaction mechanism of layered structure oxides in moist air. In 2020, Zou *et al.*[38] used $Na_{0.67}MnO_2$ and $Na_{0.67}Ni_{0.33}Mn_{0.67}O_2$ materials as the research objects to study the structural evolution in the moist environment (Fig. 3b). By using various spectroscopy and electron microscopy characterization techniques, such as XRD, solid-state NMR, TOF–SIMS, and *in situ* XRD, combined with theoretical DFT calculations, the chemical and structural changes when exposed to the ambient atmosphere were systematically studied (Fig. 3c–h). This is the first study to propose and prove that the first-cycle charging reaction potential can be used as the judgment principle for the air stability of layered oxides, which will accelerate the design, development and application of high-performance cathodes for SIBs.

4.3 Electrochemical degradation

The irreversible phase transition and water erosion occur in the layered oxide cathode, resulting in rapid capacity decay and limiting the reversible capacity. The electrochemical performance of the layered structure cathodes is still poor to meet large-scale device applications, which is affected by the following reasons. First, the transition metal ions can dissolve into the electrolyte, leading to the loss of active materials. In layered manganese-based cathode materials, the existence of Mn^{3+} will lead to the extension of the Mn–O bond in a specific direction. This asymmetry of the crystal structure leads to severe structural distortion. Vacancies are formed after Na^+ is extracted from the solid matrix, which provides spaces for H_2O/H insertion to form a protonated phase. This phenomenon could block ion transport pathways, dramatically reducing the sodium ion diffusion coefficient. For example, for the P2-phase $Na_{2/3}Mn_{0.8}Fe_{0.1}Ti_{0.1}O_2$, a pristine electrode exhibits excellent electrochemical performance, in which the capacity retention is as high as 87.7% from the second cycle, while the moisture-exposed electrode only has 70% capacity retention.[69–71]

5. Strategies for structural stabilization

In response to the three main problems mentioned earlier, researchers have made continuous efforts and explorations to obtain electrode materials with excellent performance. Here, the modification strategies are mainly summarized about elemental doping, structural modulation, surface modification and composite phase modulation. Elemental doping is often used to inhibit irreversible phase changes during material cycling, side reactions occurring between the particle surface and electrolyte can be reduced by surface coating, and the cathode material can be protected from moisture and CO_2 in the air. At the same time, we can design the structure and phase of the materials to obtain satisfactory electrode materials.

5.1 Elemental doping

Transition metal ions in Na_xTMO_2 can cause the degradation of its performance because these metal ions can undergo irreversible migration during cycling, which can cause the structural

distortion of materials and irreversible transitions. To suppress this phenomenon, doping some electrochemically active/inactive elements (such as Mg, Zn, Al, Cu and Li) into Na_xTMO_2 has been reported to be beneficial.[35,36,48,60,63,68,72–74]

5.1.1 Cationic doping. Cationic doping is effective in inhibiting the irreversible phase transition, thus improving the electrochemical performance of layered oxides. By doping, the Jahn–Teller distortion can be reduced to a certain extent, and the connection between TM and O can be improved to an extent by sharing oxygen with other stable metal elements. Thus, the movement of $TM–O_6$ octahedron is inhibited and the phase transition is suppressed. The phase transition from O′3 to O1 is suppressed by the Ca-doped P3-type $Na_xNi_{1/3}Mn_{1/3}Co_{1/3}O_2$ material at a high voltage (>4.0 V). And, the repulsive force between Ca^{2+} and transition metal ions leads to the expansion of the interlayer distance of the sodium layer, which improves the diffusion rate of sodium ions and makes it exhibit greatly improved electrochemical performance during cycling.[75] Aishuak Konarov et al.[54] introduced Co into P2-type materials by the combustion method and replaced part of Mn, which reduced in Jahn–Teller distortion caused by Mn^{3+}. The electrochemical performance of the synthesized $Na_{2/3}[Mn_{0.8}Co_{0.2}]O_2$ compound reached about 175 mA h g^{-1} (0.1 C, 26 mA g^{-1}), and maintained more than 90% of its initial capacity after 300 cycles at 0.1 C and 10 C (2.6 A g^{-1}). The stable elements share oxygen, which reduces the movement of $Mn^{3+}–O_6$ octahedron and inhibits the continuous phase transition in $Na_{2/3}[Mn_{1-x}M_x]O_2$. Meanwhile, the strong Co–O bond makes the crystal structure undergo a single-phase reaction in the repeated Na^+ de/insertion process. In situ XRD and HRTEM show that the crystal structure remains unchanged after 300 cycles. However, the toxicity, scarcity and high price of Co are the disadvantages of this doping process.[76]

Compared with O3-type oxides, P2-type materials usually have larger sodium layer spacing, which is related to higher conductivity to Na^+ in the de/intercalation process. Elemental doping is used to adjust the interlayer distance of the layered oxide crystal structure. As shown in Fig. 4a and b, Wang et al.[40] successfully introduced Mg into the Na site of $P2–Na_{0.7}[Mn_{0.6}Ni_{0.4}]O_2$ materials. On the one hand, Mg^{2+} can act as a "pillar" of the stable layered structure, which can inhibit structural collapse in the c-direction during high voltage charging and high rate cycling; on the other hand, the occupation of Mg^{2+} in the Na layer and transition metal layer can form "Na–O–Mg" and "Mg–O–Mg" bonds, resulting in ionic O 2p properties, which can distribute these O 2p states at the top of the O valence band and interact with transition metals, thus promoting reversible oxygen redox. As a result, at a high cut-off voltage (4.2 V), $Na_{0.7}Mg_{0.05}[Mn_{0.6}Ni_{0.2}Mg_{0.15}]O_2$ exhibits excellent electrochemical performance, especially at a high current rate.

5.1.2 Anionic doping. Doping different anions (such as F^-, Cl^-, and S^{x-}) has been put forward as another approach to tailor the cathode materials in LIBs.[77] Li et al.[78] demonstrated the feasibility that anions (ClO_4^-) and cations (Na^+) could be co-(de)inserted in a layered structure oxide. It was first studied in a P3 phase $Na_{0.5}Ni_{0.25}Mn_{0.75}O_2$ layered structure material.
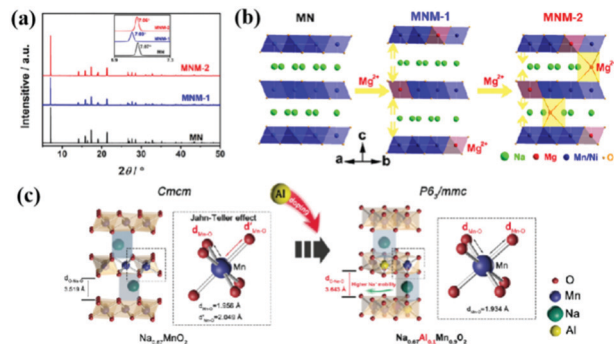

Fig. 4 (a) XRD and (b) structural evolution of Mg doped $Na_{0.7}[Mn_{0.6}Ni_{0.4-x}Mg_x]O_2$(MNM-x); adapted with permission.[40] Copyright 2018, American Chemical Society. (c) Schematic illustration of effects of Al^{3+} doping on electrode structures. Adapted with permission.[48] Copyright 2019, Wiley-VCH.

The participation of the anion provided partial charge compensation for the redox of the whole cell and the process was kinetically fast and sustainable. This proof of concept provides exciting ideas for achieving higher reversible capacities. Appropriate doping can effectively improve the ionic conductivity of the material, reduce the cation mixing, reduce the release of oxygen, inhibit the irreversible loss of oxygen, stabilize the structure of the material, and improve the cycling performance of the material.[50,79] In 2017, Zhang et al.[80] introduced F into the $O3–NaNi_{1/3}Fe_{1/3}Mn_{1/3}O_2$ material by a simple solid-state method for the first time. As a result, the rate performance and cycle performance of the material were significantly improved. Besides, F-doping is applicable in regulating the binding energy of oxygen and the ratio of Mn^{3+}/Mn^{4+} to suppress the Jahn–Teller distortion of Mn^{3+}. Besides, F-doping can increase the diffusion rate of Na^+ and improve the rate performance of the material.

Fluorination can inhibit irreversible oxygen loss and slow down the reduction of transition metal valence and structural distortion, which has been well proved in Li-rich materials.[81] Wang et al.[82] also doped non-metallic elements (F and B) into P3-type layered oxide $Na_{0.65}Mn_{0.75}Ni_{0.25}O_2$. The results show that the F-doped $Na_{0.65}Mn_{0.75}Ni_{0.25}F_{0.1}O_{1.9}$ material can significantly inhibit P3–O1 phase transition and maintain a strong M–F bond during cycling, so it shows good cycling performance. The $Na_{0.65}Mn_{0.75}Ni_{0.25}B_{0.1}O_{1.9}$ doped with B can change the P3 phase into a more stable P2 phase, thus improving the rate performance and cycle life of the material.

A suitable cation or anion may be selected to provide higher capacity to the electrode by doping to excite the redox activity of the lattice oxygen. For example, Song et al.[83] synthesized a new P3-type $Na_{2/3}Mg_{1/3}Mn_{2/3}O_2$ material using a solid-phase method. The doping of Mg^{2+} formed a strong ionic bond with oxygen, which induced the redox reaction of oxygen and provided charge compensation together with the redox reaction of transition metals to improve the energy density of sodium-ion batteries. The experimental results show that elemental doping can reduce the Jahn–Teller distortion, inhibit the phase

transition, improve the ionic conductivity of the material, and reduce the cation mixing, so as to improve the performance of the material. However, the effect of the elements doped in the materials is complicated and further study is still worthy of being done.

5.2 Micro/nano structure architecture

Poor ionic conductivity and huge volume change during cycling are common problems for bulk Na_xTMO_2 materials. These problems can be solved by adjusting the size of cathode materials and designing hollow micro/nano structures and special structures.[70,84–86]

The hollow micro/nano structure materials have high specific surface area and enough Na^+ storage sites. As a result, it can improve the rate performance and cycling stability of the cathode by effectively shortening the diffusion length of Na^+, providing buffer for the volume strain generated in the cycling process, and enhancing the ionic conductivity.[87–89] As shown in Fig. 5a–d, Lu et al.[90] prepared a shell thickness of 200 nm and a diameter of 2 μm polypyrrole-coated hollow microspheres $Na_{0.7}MnO_{2.05}$ (NMOHS@PPy). The hollow microspheres increase the contact area with the electrolyte and shorten the ion diffusion length. The diffusion coefficient of

$Na^+(D_{Na+})$ in the electrode material is improved from 7.08×10^{-13} cm^2 s^{-1} to 2.07×10^{-12} cm^2 s^{-1}. The improved electrical conductivity is related to the PPy coating, which can stabilize the hollow structure and improve the electrochemical performance. The initial capacity is 165.1 mA h g^{-1}, and the capacity retention rate reaches 88.6% after 100 cycles of 0.1 A g^{-1} and the cycle performance of NMOHS@PPy is significantly higher than that of $Na_{0.7}MnO_{2.05}$ solid microspheres (NMOSS). Hollow micro/nano structure materials can solve the problems of ionic conductivity and volume change to a certain extent, but compared with solid particles, their tap density decreases, resulting in the decrease of volume energy density. A proper balance between the bulk energy density and electrochemical performance is needed.

Generally, in order to obtain materials with higher tap density, applying spherical particles with uniform size can be a choice, because they tend to have higher volume energy density compared with irregular particles. Karthikeyan Kaliyappan et al.[91] synthesized spherical $Na_{0.66}(Ni_{0.13}Mn_{0.54}Co_{0.13})O_2$ (Na–NMC) particles with a uniform size of 5 μm by using a simple method. Urea and ethylene glycol were used to control the particle shape, uniformity and tap density. Compared with the traditional co-precipitation synthesis method, it is more

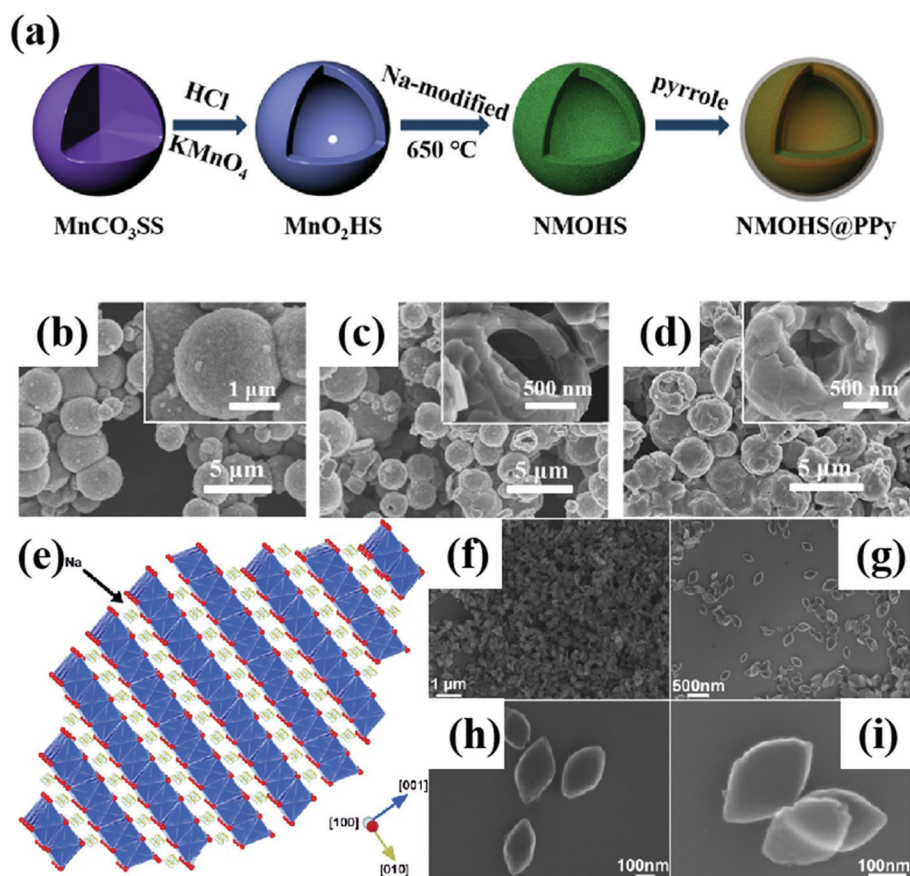Fig. 5 (a) The synthetic schematic diagram of NMOHS@PPy; SEM images of (b) MnO_2 and (c) NMOHS and (d) NMOHS@PPy hollow microspheres; adapted with permission.[90] Copyright 2019, American Chemical Society. (e) Schematic diagram of the exposed (100) crystal surface of $Na_{0.7}MnO_2$;[93] (f–i) the FESEM images of $Na_{0.7}MnO_2$ nanoplates. Adapted with permission.[93] Copyright 2013, Wiley-VCH.

convenient and practical. Na–NMC has a high tap density of 2.34 g cm^{-3}, and still exhibits good electrochemical performance at a high voltage of 4.7 V. The uniform size of the spherical particles increases the diffusion of Na$^+$, and improves the bulk energy density and cyclicity of Na–NMC.

During the cycling process, the irreversible phase transition and repeated Na$^+$ extraction/insertion of the electrode material will lead to the anisotropic change of lattice parameters, resulting in severe strain at the particle boundary and microcracks. The repeated expansion and contraction of the lattice destroy the contact among the particles, resulting in the decrease of the cycling performance and the poor rate performance of the electrode materials. The synthesis of single crystal particles provides an idea for solving intergranular cracks.[92] Compared with polycrystalline particles, single crystal materials often have better high-voltage stability. For example, Su et al.[93] synthesized a single crystal Na$_{0.7}$MnO$_2$ material with a rhombic morphology by hydrothermal method (Fig. 5e–i). The single crystal properties were confirmed by HRTEM and SAED characterization. It is designed in such a way that all the exposed faces are active (100) planes, which is more conducive to the de/intercalation of Na$^+$. The electrochemical performance results show that the material has a very high initial capacity of 164 mA h g^{-1} (Na$_{0.7}$MnO$_2$ theoretical capacity of 170 mA h g^{-1}) and shows good rate performance and cycle performance.

In addition to the size control of materials, the synthesis of hollow structure and single crystal materials, etc., one can also apply some strategies developed in LIBs to SIBs. The new progressive gradient positive materials are in full swing in LIBs, and the internal stress of the materials can be relieved by the reasonable distribution of transition metal ions. Similar to this principle, Jang-Yeon Hwang et al.[44] studied a radially aligned hierarchical columnar structure in spherical particles (RAHC particles). The structure of the material is Na[Ni$_{0.75}$Co$_{0.02}$Mn$_{0.23}$]O$_2$ inside to Na[Ni$_{0.58}$Co$_{0.06}$Mn$_{0.36}$]O$_2$ outside. From inside to outside, Ni elements continue to decrease, and Co and Mn elements continue to increase. This internal higher nickel component design can increase the discharge capacity of the material, and the external higher manganese component can improve the material stability and cycle performance. An advantage of the radial arrangement of the columnar structure is that it can improve the diffusion rate of Na$^+$. This unique structure of the cathode exhibits very good performance.

The stability, electrochemical properties and vibration density of the electrode materials are largely related to the cathode materials, including their size, morphology and structure. Hollow micro/nanostructure materials generally have high specific surface area, and better electron and ion transport. However, they tend to have intensified side reactions and lower energy density. In addition, applying materials with new structures, such as single crystals, also provides a way to improve the stability of cathode materials. However, there are still some problems in the preparation of single crystal materials, such as particle aggregation and non-uniform morphology and size.

5.3 Surface modification

In addition to the above-mentioned irreversible phase transition, low ionic conductivity and large volume strain, the

dissolution of the Na$_x$TMO$_2$ cathode material and the side reaction between the electrode material and the water and electrolyte in the air often lead to the degradation of battery performance. As an effective modification strategy, surface coating can not only improve the electronic/ionic conductivity of the material, but also protect the active part of the material from the influence of moisture and CO$_2$ in the air, and reduce the formation of insulation such as NaOH and Na$_2$CO$_3$ on the surface of the material.[55,94–96] At the same time, it can reduce the direct contact between the electrode material and electrolyte, so as to reduce the side reaction between the electrode material and electrolyte interface.

Wang et al.[97] synthesized the P3–Na$_{0.65}$Mn$_{0.75}$Ni$_{0.25}$O$_2$ material with metal phosphate coating using a co-precipitation method. Their study showed that the coating of both aluminum and magnesium phosphate positively affected the performance of the electrode material. The protective coating inhibited irreversible oxidation under high voltage conditions to some extent, thus improving the cycle life of the material. Notably, the coating also improved the air stability of the Na$_{0.65}$Mn$_{0.75}$Ni$_{0.25}$O$_2$ electrode, allowing it to maintain a high electrochemical activity when being exposed to air. Generally, the type, thickness and uniformity of the coating have a great influence on the properties of the material. When the coating is too thick or uneven, the electronic and ionic conductivity of the material will decrease. Atomic layer deposition (ALD) can be used to deposit a uniform metal oxide coating on the electrode surface. This strategy has been widely used to improve the electrochemical performance of LIBs,[98–100] and then to improve the performance of SIB cathode materials. Molecular layer deposition (MLD) is similar to ALD, and can be used to produce uniform and ultra-thin polymer or organometallic coatings. Karthikeyan Kaliyappan et al.[59] synthesized a P2-type layered cathode material (Alu–NMM) with ultra-thin polymer metal mixed coating by this method (Fig. 6a). The experimental results show that this material can maintain structural stability under high pressure. Moreover, the capacity retention of Alu–NMM is 86% after 100 cycles at 0.1 C, which is much higher than that of Na$_{0.66}$Mn$_{0.9}$Mg$_{0.1}$O$_2$ (65%) and Al$_2$O$_3$–NMM (71%) prepared by ALD. This can be attributed to the higher electronic/ionic conductivity and flexibility of Alu–NMM.

In contrast to the general coating strategy, Guo et al. synthesized cathode oxide materials with elemental doping-induced surface reconstruction by a simple solid-phase method (Fig. 5b).[101] An atomic scale interface composed of spinel titanium oxide was formed by introducing Ti^{4+}. This unique surface improves the structural stability and ionic conductivity of NaMnTi$_{0.1}$Ni$_{0.1}$O$_2$ (NMTN). Only 36% of the capacity of NaMnO$_2$ (NM) remains after 50 cycles at a 0.5 C rate. By contrast, 85% of the capacity of NMTN remains after 100 cycles (Fig. 5c). The NMTN electrodes exhibit excellent electrochemical properties as seen in Fig. 5d–g. Surface reconstruction has been proved to be a useful approach to improve the performance of cathode materials.

Surface coating, like elemental doping, has been widely studied as a simple and effective modification method to
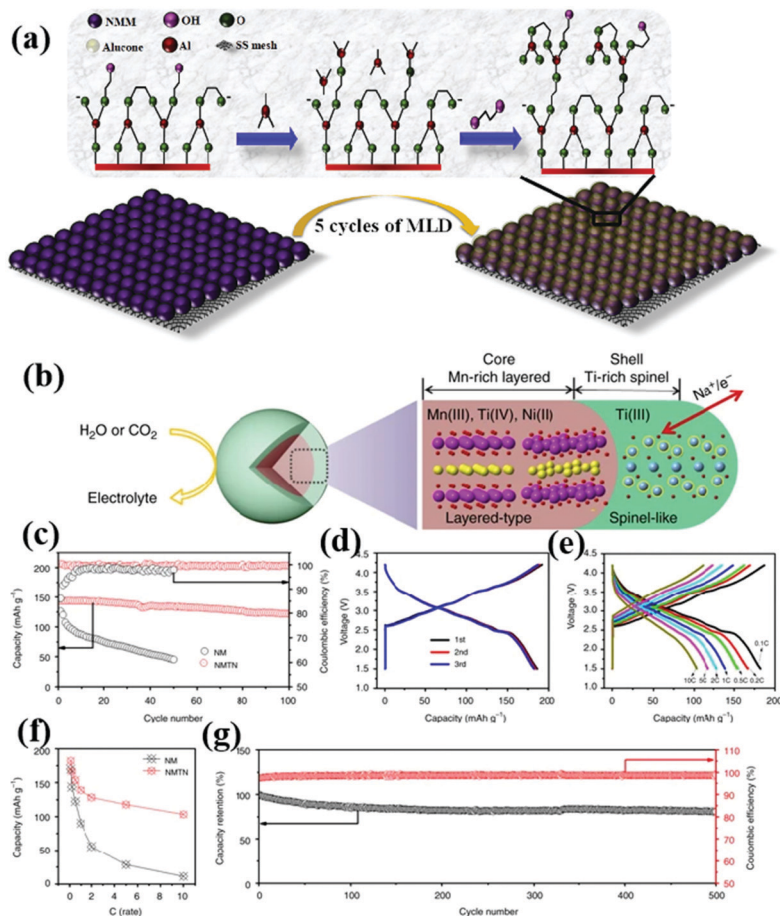
Fig. 6 (a) MLD process of NMM powder surface; adapted with permission.[59] Copyright 2020, Wiley-VCH. (b) Three-dimensional structure model of an NMTN sample composed of a Ti-rich spinel-like interface (green shell) and a Mn-rich layered body (brown core);[101] electrochemical performance diagrams of NM and NMTN: (c) 0.5 C cycle performance diagram;[101] (d) rate performance diagram, (e) 0.1 C charge and discharge curve, (f) charge and discharge curves at different rates and (g) 5 C cycle performance graph and coulombic efficiency graph. Adapted with permission.[101] Copyright 2017, All Rights Reserved.

optimize the performance of cathode materials. However, surface coating is generally used to reduce the side reactions on the surface of electrode materials, which cannot inhibit irreversible phase transition and structural volume change during the charge discharge process. Therefore, the combination of elemental doping and surface coating is usually used to improve the electrochemical performance of sodium-based cathode materials.

5.4 Chemical phase compositions

Materials with P2, P3 and O3 phases are the most studied so far. Generally, the diffusion rate of Na$^+$ in P2-type materials is higher, but the initial coulombic efficiency is lower due to the irreversible phase transition. The interlayer spacing for P3 type is larger than that of P2 phase materials, which provides a wider path for Na$^+$ diffusion, thus showing the improved rate performance. O3-type structural materials have higher sodium content, but the diffusion speed of the P2 type Na$^+$ is slower, resulting in a unsatisfactory cycle performance. Therefore, researchers have been committed to studying better structures to obtain excellent electrochemical performance. A composite

material is obtained by combining the advantages of different phases, which provides a new way to obtain new cathodes with excellent performance.

For example, Yang et al.[31] studied a Co- and Ni-free P2/O3 biphase Na$_{0.8}$Li$_{0.2}$Fe$_{0.2}$Mn$_{0.6}$O$_2$ material, which is composed of O3 and P2/O3 crystals (Fig. 7a). 95% of Li exists in the transition metal layer and acts as a structural stabilizer. XRD and TEM analyses show that the material is biphasic, and the initial reversible capacity of the material is 174 mA h g^{-1} with 82% capacity retention, which can be attributed to the contribution of Fe^{3+}/Fe^{4+}, oxygen and partial Mn$^{3+/4+}$ redox. In addition to P2/O3 composite materials,[102,103] there are P2/P3 phase,[32] P2/tunnel structure and so on (Fig. 7b–d).[104,105] By using the unique advantages of different phases to synergize them, it opens up a new field for improving the properties of Na$_x$TMO$_2$ materials. Although this modification strategy has some advantages, the preparation of more composite materials and the mechanism of the interactions between different phases need to be further studied.

Through the chemical composition control, structure design and surface modification of Na$_x$TMO$_2$ materials, the problems
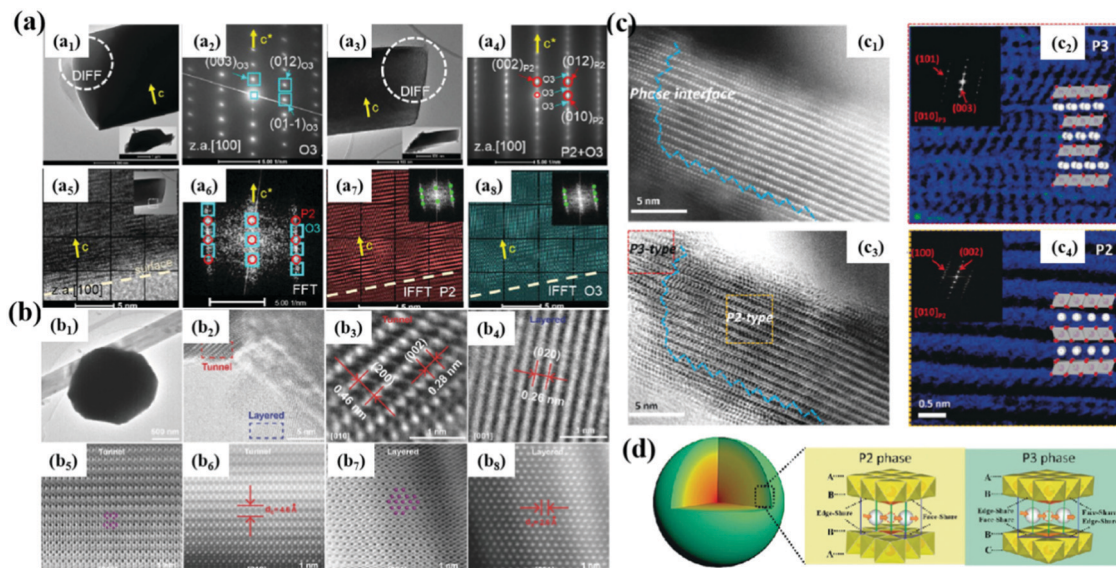
Fig. 7 (a) TEM, SAED, FFT and IFFT patterns of P2/O3 biphase $Na_{0.8}Li_{0.2}Fe_{0.2}Mn_{0.6}O_2$; adapted with permission.[31] Copyright 2020, Wiley-VCH. (b) TEM, HR-TEM, HAADF-STEM and ABF-STEM images of layer/tunnel structure materials;[104] (c) HAADF and ABF images of P2@P3NCZM composite material; adapted with permission.[103] Copyright 2018, Wiley-VCH. (d) 3D structural model of the NCZM samples composed of P3 and P2 with the corresponding Na-ion migration paths in different layered structures. Adapted with permission.[103] Copyright 2019, Wiley-VCH.

of irreversible phase transition, instability and poor electrochemical performance of the materials in the cycle process can be solved. Based on the synergistic effect, we can reasonably use a number of methods to improve the performance of the electrode, and the most commonly used method is the combination of doping and coating.[106,107] Gaining an in-depth understanding of the cause of these issues is also essential for eventually addressing them. For example, the sodium-deficient layered P3-phase $Na_{0.5}Mg_{0.15}Al_{0.2}Mn_{0.65}O_2$ electrode was selected for investigation by Jia *et al.*[108] The structural evolution of the material during cycling, the source of irreversible oxygen release and the whole anion redox process were elaborated by using characterization techniques such as X-ray photoelectron spectroscopy, X-ray absorption spectroscopy, and Raman and differential electrochemical mass spectrometry. Such a type of investigation provides useful insights into the design of anion redox-based batteries. Here, Table 2 briefly summarizes the electrochemical performance of sodium-ion batteries with different transition metal oxides synthesized by different modification methods. Moreover, it is significant to use advanced characterization techniques to determine the reaction mechanism of transition metal ions in the cycling process.[38,109,110]

6. Summary and perspectives

Generally speaking, as the most promising alternative product of LIBs, there are still many problems remaining in the commercialization of SIBs. It is particularly notable in terms of energy density, where there is much room for improvement. In the process of improving battery energy density, the

preparation of cathode and anode materials for batteries is no doubt vitally important. In terms of cathode materials, the energy density of sodium-ion batteries has become comparable to that of lithium-ion batteries such as lithium iron phosphate; however, it is still far below the high-nickel high-voltage ternary materials or lithium-rich manganese-based cathode materials, making it difficult to being applied in the field of power batteries. However, sodium-ion batteries exhibit a high-cost performance and are expected to play a big role in the field of energy storage. In order to achieve such a goal, improving the energy density and cycle life of the material is becoming the major effort of the current investigation of sodium-ion batteries. Layered transition metal oxides have attracted much attention due to their high capacity, easy synthesis and similar chemical reactions with LIB cathode analogues. However, there are many problems in the charge/discharge process of Na_xTMO_2, such as complex phase transition and the dissolution and migration of transition metal ions.

The elemental doping in Na_xTMO_2 can suppress the Jahn–Teller distortion of the material and mitigate the irreversible phase transitions that induce large electrochemical degradations. Reasonably designed morphology and microstructure can improve the diffusion kinetics of Na^+ and ion conductivity. For example, spherical particles of uniform size can increase the tap density of the material and increase the volume energy density. At the same time, the ALD/MLD method can be used to obtain a uniform coating to prevent the dissolution of the P2 layered cathode material. The instability of the transition metal oxide in a humid environment can also be relieved by surface modification to reduce the formation of insulating residues on the surface of the material, so as to improve the stability and cycle performance of the material. In addition, some unique

View Article Online

Nanoscale Horizons   Review

Table 2 Summary of the properties of different transition metal oxides synthesized using various modification strategies

Materials	Phase	Voltage range [V]	Discharge capacity [mA h g^{-1}]/ current density [mA g^{-1}]	Capacity retention (%)/number of cycles	Strategies for structural stabilization	Ref.
$Na_{0.6}MnO_2$	Layered–tunnel structure	1.5–4.3	198.2/40	85.1/100	Structure architecture	104
$Na_{2/3}MnO_2$	P2	2.0–3.8	170/12	100/50	Structure architecture	84
$Na_{0.7}MnO_{2.05}$@PPy	P2	1.8–4.4	165.1/100	88.6/100	Structure architecture; surface modification	90
$Na_{0.7}MnO_2$	Single crystalline	2–4.5	163/40	94/10	Structure architecture	93
Sn–Na[$Ni_{0.5}Mn_{0.5}$]O_2	O3	2.0–4.0	144.3/15	84.9/100	Surface modification	46
$Na_{0.5}Ni_{0.25}Mn_{0.75}O_2$	P3	3.75–4.25	180/20	85/100	Elemental doping	78
$NaNi_{0.5}Mn_{0.5}O_2$	O3	2.0–4.0	133/9.375	70.0/500	Structure architecture	89
$Na_{2/3}Zn_{1/4}Mn_{3/4}O_2$	P2	1.5–4.5	202.4/20	67/50	Elemental doping	63
Al_2O_3@$Na_{0.67}Zn_{0.1}Mn_{0.9}O_2$	P2	2.0–4.4	155/12	83/100	Surface modification	107
$Na_{0.612}K_{0.056}MnO_2$	P2	1.8–4.3	240.5/20	98.2/100	Elemental doping	35
Alucone-coated $Na_{0.66}Mn_{0.9}Mg_{0.1}O_2$	P2	2–4.5	163.1/200	86/100	Surface modification	59
$AlPO_4$-coated $Na_{0.65}Mn_{0.75}Ni_{0.25}O_2$	P3	1.5–4.2	179.4/17	61.5/100	Surface modification	97
Na[$Ni_{2/3}Ru_{1/3}$]O_2	O3	2–4.1	154/10.5	$\approx$79/200	Elemental doping	34
$NaNi_{2/3}Ru_{1/3}O_2$	O3	2–3.8	130/5	81/1000	Structure architecture	111
$Na_{2/3}$[$Mn_{0.8}Co_{0.2}$]O_2	P2	1.5–4.6	175/26	90/300	Elemental doping	54
$Na_{0.5}Mg_{0.15}Al_{0.2}Mn_{0.65}O_2$	P3	2–4.5	177/10	$\approx$82/100	Elemental doping	108
RAHC-Na[$Ni_{0.6}Co_{0.05}Mn_{0.35}$]$O_2$	O3	1.5–3.9	157/15	84/100	Structure architecture	44
$Na_{0.66}$($Ni_{0.13}Mn_{0.54}Co_{0.13}$)$O_2$	P2	2–4.7	121/200	90/150	Structure architecture	91
$Na_{0.67}Ni_{0.28}Mg_{0.05}Mn_{0.67}O_2$@$NaTi_2(PO_4)_3$	P2	2.5–4.3	130.4/17.3	77.4/200	Elemental doping; surface modification	112
$Na_{2/3}$[($Ni_{0.5}Zn_{0.5}$)$_{0.3}Mn_{0.7}$]O_2	P2	2.3–4.6	130/26	95/200	Elemental doping	53
$Na_{0.67}$[$Li_{0.21}Mn_{0.59}Ti_{0.2}$]$O_2$	P2	1.5–4.5	231/20	—	Elemental doping	36
$Na_{0.8}Li_{0.2}Fe_{0.2}Mn_{0.6}O_2$	P2/O3	2.0–4.6	174/15	82/100	Chemical phase compositions	31
$Na_{0.67}$[$Ni_{0.1}Fe_{0.1}Mn_{0.8}$]O_2	P′2	1.5–4.3	$\approx$220/13	80/200	Elemental doping	51
$Na_{0.78}Cu_{0.27}Zn_{0.06}Mn_{0.67}O_2$	P2@P3	2.5–4.1	84/100	85/200	Chemical phase compositions	103
$NaMnTi_{0.1}Ni_{0.1}O_2$	P2/O′3	1.5–4.2	186/20	81/500	Elemental doping; surface modification	101
ZrO_2@$NaNi_{0.7}Mn_{0.15}Co_{0.15}O_2$	O3	1.5–3.9	125.5/0.1 C	—	Surface modification	113
$Na_{0.7}Li_{0.06}Mg_{0.06}Ni_{0.22}Mn_{0.67}O_2$	P2/P3	2.0–4.4	129/24	97.2/50	Chemical phase compositions	32
$Na_{0.52}Ca_{0.04}Ni_{2/3}Mn_{2/3}Co_{2/3}O_2$	P3	2.5–4.2	173/10	77/105	Elemental doping	75
$Na_{0.8}$[($Ni_{0.5}Co_{0.2}Mn_{0.3}$)$_{0.6}$($Ni_{0.33}Mn_{0.67}$)$_{0.4}$]O_2	O3/O′3–P2	1.5–4.0	146/15	$\approx$75/200	Structure architecture; chemical phase compositions	42
$NaNi_{0.12}Cu_{0.12}Mg_{0.12}Fe_{0.15}Co_{0.15}Mn_{0.1}Ti_{0.1}Sn_{0.1}Sb_{0.04}O_2$	O3	2.0–3.9	110/12	83/500	Elemental doping, Structure architecture	37

structures have recently been developed, such as two-phase composite structures, concentration gradient structures, and core–shell structures to improve the electrochemical performance of the material. A number of studies have shown that it could stimulate the anion redox activity in Na_xTMO_2 to provide additional capacity beyond the definite capacity provided by the original cation. However, due to the large difference in the size between NaO_6 and MO_6 octahedra, it is not so easy to realize the redox activity of anions.

Therefore, to develop state-of-the-art cathode materials, it is necessary to reveal the underlying reaction mechanisms. In addition, other parts in a battery system such as the anode, electrolyte, separator, and binder also need to be further optimized. We should not only modify the existing inactive materials, but the development of new inactive materials should also draw our attention. One needs to take into account the performance of the materials individually and the compatibility between different materials for decision making. Two of the effective routes for improving the energy density are to improve the potential difference between the positive and negative electrodes and the specific capacity of the material. Therefore, the new research can start from these two aspects. For example, providing higher discharge capacity through oxygen redox, developing high-voltage materials, *etc.*, all contribute to improving the energy density of batteries. Scientists are constantly optimizing the existing materials, searching for new materials, and optimizing manufacturing techniques to obtain higher energy density batteries. Despite facing many severe challenges, layered oxide materials still have great commercial prospects as cathode materials for SIBs.

Conflicts of interest

The authors declare no competing financial interest.

Acknowledgements

This work was supported by the National Natural Science Foundation of China (51872209 and 51972239), the Zhejiang

348 | *Nanoscale Horiz.*, 2022, **7**, 338–351   This journal is © The Royal Society of Chemistry 2022

References

1 D. Yang, D. Chen, Y. Jiang, E. H. Ang, Y. Feng, X. Rui and Y. Yu, *Carbon Energy*, 2020, **3**, 50–65.

2 X. Zhang, S. Pan, H. Song, W. Guo, F. Gu, C. Yan, H. Jin, L. Zhang, Y. Chen and S. Wang, *J. Mater. Chem. A*, 2021, **9**, 19734–19740, DOI: 10.1039/d1ta03652a.

3 A. Eftekhari and D.-W. Kim, *J. Power Sources*, 2018, **395**, 336–348.

4 M. Bianchini, M. Roca-Ayats, P. Hartmann, T. Brezesinski and J. Janek, *Angew. Chem., Int. Ed.*, 2019, **58**, 10434–10458.

5 Q. Tao, L. Wang, C. Shi, J. Li, G. Chen, Z. Xue, J. Wang, S. Wang and H. Jin, *Mater. Chem. Front.*, 2021, **5**, 2607–2622.

6 X. Yan, L. Lin, Q. Chen, Q. Xie, B. Qu, L. Wang and D. L. Peng, *Carbon Energy*, 2021, **3**, 303–329.

7 L. Wang, T. Liu, A. Dai, V. De Andrade, Y. Ren, W. Xu, S. Lee, Q. Zhang, L. Gu, S. Wang, T. Wu, H. Jin and J. Lu, *Nat. Commun.*, 2021, **12**, 5370.

8 D. Lin, Y. Liu and Y. Cui, *Nat. Nanotechnol.*, 2017, **12**, 194–206.

9 P. K. Nayak, L. Yang, W. Brehm and P. Adelhelm, *Angew. Chem., Int. Ed.*, 2018, **57**, 102–120.

10 P. Wang, Y. You, Y. Yin and Y. Guo, *Adv. Energy Mater.*, 2018, **8**, 1701912.

11 H. Liu, W. Deng, X. Gao, J. Chen, S. Yin, L. Yang, G. Zou, H. Hou and X. Ji, *Nano Sel.*, 2020, **1**, 200–225.

12 Y. Xiao, N. M. Abbasi, Y. F. Zhu, S. Li, S. J. Tan, W. Ling, L. Peng, T. Yang, L. Wang, X. D. Guo, Y. X. Yin, H. Zhang and Y. G. Guo, *Adv. Funct. Mater.*, 2020, **30**, 2001334.

13 Q. Liu, Z. Hu, W. Li, C. Zou, H. Jin, S. Wang, S. Chou and S.-X. Dou, *Energy Environ. Sci.*, 2021, **14**, 158–179.

14 G. Yao, X. Zhang, Y. Yan, J. Zhang, K. Song, J. Shi, L. Mi, J. Zheng, X. Feng and W. Chen, *J. Energy Chem.*, 2020, **50**, 387–394.

15 M. Chen, W. Hua, J. Xiao, D. Cortie, W. Chen, E. Wang, Z. Hu, Q. Gu, X. Wang, S. Indris, S. L. Chou and S. X. Dou, *Nat. Commun.*, 2019, **10**, 1480.

16 Q. Ni, Y. Bai, F. Wu and C. Wu, *Adv. Sci.*, 2017, **4**, 1600275.

17 Y. Lu, L. Wang, J. Cheng and J. B. Goodenough, *Chem. Commun.*, 2012, **48**, 6544–6546.

18 Q. Liu, Z. Hu, M. Chen, C. Zou, H. Jin, S. Wang, S.-L. Chou, Y. Liu and S. X. Dou, *Adv. Funct. Mater.*, 2020, **30**, 1909530.

19 B. Xie, P. Zuo, L. Wang, J. Wang, H. Huo, M. He, J. Shu, H. Li, S. Lou and G. Yin, *Nano Energy*, 2019, **61**, 201–210.

20 J. Sun, H. Ye, J. A. S. Oh, Y. Sun, A. Plewa, Y. Wang, T. Wu, K. Zeng and L. Lu, *Nano Res.*, 2021, DOI: 10.1007/s12274-021-3844-7.

21 S. Xu, Y. Wang, L. Ben, Y. Lyu, N. Song, Z. Yang, Y. Li, L. Mu, H. Yang, L. Gu, Y. Hu, H. Li, Z. Cheng, L. Chen and X. Huang, *Adv. Energy Mater.*, 2015, **5**, 1501156.

22 Y. Wang, J. Liu, B. Lee, R. Qiao, Z. Yang, S. Xu, X. Yu, L. Gu, Y. S. Hu, W. Yang, K. Kang, H. Li, X. Q. Yang, L. Chen and X. Huang, *Nat. Commun.*, 2015, **6**, 6401.

23 X. L. Li, T. Wang, Y. Yuan, X. Y. Yue, Q. C. Wang, J. Y. Wang, J. Zhong, R. Q. Lin, Y. Yao, X. J. Wu, X. Q. Yu, Z. W. Fu, Y. Y. Xia, X. Q. Yang, T. Liu, K. Amine, Z. Shadike, Y. N. Zhou and J. Lu, *Adv. Mater.*, 2021, **33**, e2008194.

24 Y. Yang and W.-F. Wei, *Rare Met.*, 2020, **39**, 332–334.

25 C. Delmas, C. Fouassier and P. Hagenmuller, *Physica*, 1980, **99**, 81–85.

26 Q. Liu, Z. Hu, M. Chen, C. Zou, H. Jin, S. Wang, S. L. Chou and S. X. Dou, *Small*, 2019, **15**, 1805381.

27 Y. N. Zhou, P. F. Wang, X. D. Zhang, L. B. Huang, W. P. Wang, Y. X. Yin, S. Xu and Y. G. Guo, *ACS Appl. Mater. Interfaces*, 2019, **11**, 24184–24191.

28 T. Risthaus, L. Chen, J. Wang, J. Li, D. Zhou, L. Zhang, D. Ning, X. Cao, X. Zhang, G. Schumacher, M. Winter, E. Paillard and J. Li, *Chem. Mater.*, 2019, **31**, 5376–5383.

29 L. Zhang, J. Wang, G. Schuck, F. Xi, L. Du, M. Winter, G. Schumacher and J. Li, *Small Methods*, 2020, **4**, 2000422.

30 Y. F. Zhu, Y. Xiao, W. B. Hua, S. Indris, S. X. Dou, Y. G. Guo and S. L. Chou, *Angew. Chem., Int. Ed.*, 2020, **59**, 9299–9304.

31 L. Yang, J. M. L. Amo, Z. Shadike, S. M. Bak, F. Bonilla, M. Galceran, P. K. Nayak, J. R. Buchheim, X. Q. Yang, T. Rojo and P. Adelhelm, *Adv. Funct. Mater.*, 2020, **30**, 2003364.

32 Y. Zhou, P. Wang, Y. Niu, Q. Li, X. Yu, Y. Yin, S. Xu and Y. Guo, *Nano Energy*, 2019, **55**, 143–150.

33 C. Zhao, Q. Wang, Z. Yao, J. Wang, B. Sánchez-Lengeling, F. Ding, X. Qi, Y. Lu, X. Bai and B. Li, *Science*, 2020, **370**, 708–711.

34 N. Voronina, N. Yaqoob, H. J. Kim, K. S. Lee, H. D. Lim, H. G. Jung, O. Guillon, P. Kaghazchi and S. T. Myung, *Adv. Energy Mater.*, 2021, **11**, 2100901.

35 C. Wang, L. Liu, S. Zhao, Y. Liu, Y. Yang, H. Yu, S. Lee, G. H. Lee, Y. M. Kang, R. Liu, F. Li and J. Chen, *Nat. Commun.*, 2021, **12**, 2256.

36 H. Xu, C. Cheng, S. Chu, X. Zhang, J. Wu, L. Zhang, S. Guo and H. Zhou, *Adv. Funct. Mater.*, 2020, **30**, 2005164.

37 C. Zhao, F. Ding, Y. Lu, L. Chen and Y. S. Hu, *Angew. Chem., Int. Ed.*, 2020, **59**, 264–269.

38 W. Zuo, J. Qiu, X. Liu, F. Ren, H. Liu, H. He, C. Luo, J. Li, G. F. Ortiz, H. Duan, J. Liu, M. S. Wang, Y. Li, R. Fu and Y. Yang, *Nat. Commun.*, 2020, **11**, 3544.

39 H. R. Yao, P. F. Wang, Y. Gong, J. Zhang, X. Yu, L. Gu, C. OuYang, Y. X. Yin, E. Hu, X. Q. Yang, E. Stavitski, Y. G. Guo and L. J. Wan, *J. Am. Chem. Soc.*, 2017, **139**, 8440–8443.

40 Q. C. Wang, J. K. Meng, X. Y. Yue, Q. Q. Qiu, Y. Song, X. J. Wu, Z. W. Fu, Y. Y. Xia, Z. Shadike, J. Wu, X. Q. Yang and Y. N. Zhou, *J. Am. Chem. Soc.*, 2019, **141**, 840–848.

41 M. Bianchini, J. Wang, R. J. Clement, B. Ouyang, P. Xiao, D. Kitchaev, T. Shi, Y. Zhang, Y. Wang, H. Kim, M. Zhang, J. Bai, F. Wang, W. Sun and G. Ceder, *Nat. Mater.*, 2020, **19**, 1088–1095.

42 C. Chen, Z. Han, S. Chen, S. Qi, X. Lan, C. Zhang, L. Chen, P. Wang and W. Wei, *ACS Appl. Mater. Interfaces*, 2020, **12**, 7144–7152.

43 C. Hakim, N. Sabi, L. A. Ma, M. Dahbi, D. Brandell, K. Edström, L. C. Duda, I. Saadoune and R. Younesi, *Commun. Chem.*, 2020, **3**, 1–9.

44 J. Y. Hwang, S. M. Oh, S. T. Myung, K. Y. Chung, I. Belharouak and Y. K. Sun, *Nat. Commun.*, 2015, **6**, 6865.

45 L. Mu, X. Feng, R. Kou, Y. Zhang, H. Guo, C. Tian, C. J. Sun, X. W. Du, D. Nordlund, H. L. Xin and F. Lin, *Adv. Energy Mater.*, 2018, **8**, 1801975.

46 H. H. Ryu, G. Han, T. Y. Yu and Y. K. Sun, *J. Phys. Chem. C*, 2021, **125**, 6593–6600.

47 H. H. Sun, J. Y. Hwang, C. S. Yoon, A. Heller and C. B. Mullins, *ACS Nano*, 2018, **12**, 12912–12922.

48 X. Liu, W. Zuo, B. Zheng, Y. Xiang, K. Zhou, Z. Xiao, P. Shan, J. Shi, Q. Li, G. Zhong, R. Fu and Y. Yang, *Angew. Chem., Int. Ed.*, 2019, **58**, 18086–18095.

49 K. Kaliyappan, J. Liu, B. Xiao, A. Lushington, R. Li, T.-K. Sham and X. Sun, *Adv. Funct. Mater.*, 2017, **27**, 1701870.

50 Y. Zhang, M. Wu, J. Ma, G. Wei, Y. Ling, R. Zhang and Y. Huang, *ACS Cent. Sci.*, 2020, **6**, 232–240.

51 J. U. Choi, J. H. Jo, Y. J. Park, K. S. Lee and S. T. Myung, *Adv. Energy Mater.*, 2020, **10**, 2001346.

52 A. Konarov, J. H. Jo, J. U. Choi, Z. Bakenov, H. Yashiro, J. Kim and S.-T. Myung, *Nano Energy*, 2019, **59**, 197–206.

53 A. Konarov, H. J. Kim, J. H. Jo, N. Voronina, Y. Lee, Z. Bakenov, J. Kim and S. T. Myung, *Adv. Energy Mater.*, 2020, **10**, 2001111.

54 A. Konarov, H. J. Kim, N. Voronina, Z. Bakenov and S. T. Myung, *ACS Appl. Mater. Interfaces*, 2019, **11**, 28928–28933.

55 J. H. Jo, J. U. Choi, A. Konarov, H. Yashiro, S. Yuan, L. Shi, Y.-K. Sun and S.-T. Myung, *Adv. Funct. Mater.*, 2018, **28**, 1705968.

56 G. Xu, R. Amine, Y. Xu, J. Liu, J. Gim, T. Ma, Y. Ren, C. Sun, Y. Liu, X. Zhang, S. M. Heald, A. Solhy, I. Saadoune, W. L. Mattis, S. Sun, Z. Chen and K. Amine, *Energy Environ. Sci.*, 2017, **10**, 1677–1693.

57 Y. Xiao, P. F. Wang, Y. X. Yin, Y. F. Zhu, Y. B. Niu, X. D. Zhang, J. Zhang, X. Yu, X. D. Guo, B. H. Zhong and Y. G. Guo, *Adv. Mater.*, 2018, **30**, 1803765.

58 Y. Xiao, Y. F. Zhu, H. R. Yao, P. F. Wang, X. D. Zhang, H. Li, X. Yang, L. Gu, Y. C. Li, T. Wang, Y. X. Yin, X. D. Guo, B. H. Zhong and Y. G. Guo, *Adv. Energy Mater.*, 2019, **9**, 1803978.

59 K. Kaliyappan, T. Or, Y. P. Deng, Y. Hu, Z. Bai and Z. Chen, *Adv. Funct. Mater.*, 2020, **30**, 1910251.

60 D. Pahari and S. Puravankara, *J. Power Sources*, 2020, **455**, 227957.

61 H. Yao, P. Wang, Y. Wang, X. Yu, Y. Yin and Y. Guo, *Adv. Energy Mater.*, 2017, **7**, 1700189.

62 L. Wang, J. Wang, X. Zhang, Y. Ren, P. Zuo, G. Yin and J. Wang, *Nano Energy*, 2017, **34**, 215–223.

63 Y. Wang, L. Wang, H. Zhu, J. Chu, Y. Fang, L. Wu, L. Huang, Y. Ren, C. J. Sun, Q. Liu, X. Ai, H. Yang and Y. Cao, *Adv. Funct. Mater.*, 2020, **30**, 1910327.

64 S. Komaba, N. Yabuuchi, T. Nakayama, A. Ogata, T. Ishikawa and I. Nakai, *Inorg. Chem.*, 2012, **51**, 6211–6220.

65 K. Wang, P. Yan and M. Sui, *Nano Energy*, 2018, **54**, 148–155.

66 L. Wang, J. Wang, F. Guo, L. Ma, Y. Ren, T. Wu, P. Zuo, G. Yin and J. Wang, *Nano Energy*, 2018, **43**, 184–191.

67 Q. Liu, Z. Hu, M. Chen, C. Zou, H. Jin, S. Wang, Q. Gu and S. Chou, *J. Mater. Chem. A*, 2019, **7**, 9215–9221.

68 L. Wang, Y. Sun, L. Hu, J. Piao, J. Guo, A. Manthiram, J. Ma and A. Cao, *J. Mater. Chem. A*, 2017, **5**, 8752–8761.

69 N. Yabuuchi, M. Kajiyama, J. Iwatate, H. Nishikawa, S. Hitomi, R. Okuyama, R. Usui, Y. Yamada and S. Komaba, *Nat. Mater.*, 2012, **11**, 512–517.

70 M. J. Aragón, P. Lavela, G. Ortiz, R. Alcántara and J. L. Tirado, *J. Alloys Compd.*, 2017, **724**, 465–473.

71 M. H. Han, E. Gonzalo, N. Sharma, J. M. López del Amo, M. Armand, M. Avdeev, J. J. Saiz Garitaonandia and T. Rojo, *Chem. Mater.*, 2015, **28**, 106–116.

72 B. Zhang, B. Zhang, L. Wang, X. Chen, Y. Lu, B. Xu and W. Yang, *J. Alloys Compd.*, 2020, **824**, 153938.

73 L. Wang, A. Dai, W. Xu, S. Lee, W. Cha, R. Harder, T. Liu, Y. Ren, G. Yin, P. Zuo, J. Wang, J. Lu and J. Wang, *J. Am. Chem. Soc.*, 2020, **142**, 14966–14973.

74 K. Wang, H. Wan, P. Yan, X. Chen, J. Fu, Z. Liu, H. Deng, F. Gao and M. Sui, *Adv. Mater.*, 2019, **31**, e1904816.

75 M. Matsui, F. Mizukoshi, H. Hasegawa and N. Imanishi, *J. Power Sources*, 2021, **485**.

76 Y. Zhu, X. Qi, X. Chen, X. Zhou, X. Zhang, J. Wei, Y. Hu and Z. Zhou, *J. Mater. Chem. A*, 2016, **4**, 11103–11109.

77 P. Vanaphuti, S. Bong, L. Ma, S. Ehrlich and Y. Wang, *ACS Appl. Energy Mater.*, 2020, **3**, 4852–4859.

78 Q. Li, Y. Qiao, S. Guo, K. Jiang, Q. Li, J. Wu and H. Zhou, *Joule*, 2018, **2**, 1134–1145.

79 W. Zheng, Q. Liu, Z. Wang, Z. Wu, S. Gu, L. Cao, K. Zhang, J. Fransaer and Z. Lu, *Energy Storage Mater.*, 2020, **28**, 300–306.

80 Q. Zhang, Y. Huang, Y. Liu, S. Sun, K. Wang, Y. Li, X. Li, J. Han and Y. Huang, *Sci. China Mater.*, 2017, **60**, 629–636.

81 Y. Pei, S. Li, Q. Chen, R. Liang, M. Li, R. Gao, D. Ren, Y.-P. Deng, H. Jin, S. Wang, D. Su, Y. Hu and Z. Chen, *J. Mater. Chem. A*, 2021, **9**, 2325–2333.

82 Y. Wang, X. Wang, X. Li, R. Yu, M. Chen, K. Tang and X. Zhang, *Chem. Eng. J.*, 2019, **360**, 139–147.

83 B. Song, E. Hu, J. Liu, Y. Zhang, X.-Q. Yang, J. Nanda, A. Huq and K. Page, *J. Mater. Chem. A*, 2019, **7**, 1491–1498.

84 E. Jung, Y. Park, K. Park, M. S. Kwon, M. Park, A. K. Sinha, B. H. Lee, J. Kim, H. S. Lee, S. I. Chae, S. P. Cho, K. T. Lee and T. Hyeon, *Chem. Commun.*, 2019, **55**, 4757–4760.

85 B. Peng, Z. Sun, L. Zhao, J. Li and G. Zhang, *Energy Storage Mater.*, 2021, **35**, 620–629.

86 J. Hao, K. Xiong, J. Zhou, A. M. Rao, X. Wang, H. Liu and B. Lu, *Energy Environ. Mater.*, 2022, **5**, 261–269.

87 X. Liu, W. Lai and S. Chou, *Mater. Chem. Front.*, 2020, **4**, 1289–1303.

88 J. Liu, Y. Yuan, X. Guo, B. Li, R. Shahbazian-Yassar, D. H. Liu, Z. Chen, K. Amine, J. Lu, L. Yang and Z. Bai, *Adv. Energy Mater.*, 2021, **11**, 2100503.

89 Q. Mao, R. Gao, Q. Li, D. Ning, D. Zhou, G. Schuck, G. Schumacher, Y. Hao and X. Liu, *Chem. Eng. J.*, 2020, **382**, 122978.

90 D. Lu, Z. Yao, Y. Zhong, X. Wang, X. Xia, C. Gu, J. Wu and J. Tu, *ACS Appl. Mater. Interfaces*, 2019, **11**, 15630–15637.

91 K. Kaliyappan, W. Xaio, T.-K. Sham and X. Sun, *Adv. Funct. Mater.*, 2018, **28**, 1801898.

92 X. Xu, H. Huo, J. Jian, L. Wang, H. Zhu, S. Xu, X. He, G. Yin, C. Du and X. Sun, *Adv. Energy Mater.*, 2019, **9**, 1803963.

93 D. Su, C. Wang, H.-J. Ahn and G. Wang, *Chem. – Eur. J.*, 2013, **19**, 10884–10889.

94 T. Song and E. Kendrick, *J. Phys. Mater.*, 2021, **4**, 032004.

95 Y. Han, S. Heng, Y. Wang, Q. Qu and H. Zheng, *ACS Energy Lett.*, 2020, **5**, 2421–2433.

96 L. Wang, P. Zuo, G. Yin, Y. Ma, X. Cheng, C. Du and Y. Gao, *J. Mater. Chem. A*, 2015, **3**, 1569–1579.

97 Y. Wang, K. Tang, X. Li, R. Yu, X. Zhang, Y. Huang, G. Chen, S. Jamil, S. Cao, X. Xie, Z. Luo and X. Wang, *Chem. Eng. J.*, 2019, **372**, 1066–1076.

98 X. Meng, X. Q. Yang and X. Sun, *Adv. Mater.*, 2012, **24**, 3589–3615.

99 Y. Liu, X. Wang, J. Cai, X. Han, D. Geng, J. Li and X. Meng, *J. Mater. Sci. Technol.*, 2020, **54**, 77–86.

100 X. Meng, *Energy Storage Mater.*, 2020, **30**, 296–328.

101 S. Guo, Q. Li, P. Liu, M. Chen and H. Zhou, *Nat. Commun.*, 2017, **8**, 135.

102 E. Lee, J. Lu, Y. Ren, X. Luo, X. Zhang, J. Wen, D. Miller, A. DeWahl, S. Hackney, B. Key, D. Kim, M. D. Slater and C. S. Johnson, *Adv. Energy Mater.*, 2014, **4**, 1400458.

103 Z. Yan, L. Tang, Y. Huang, W. Hua, Y. Wang, R. Liu, Q. Gu, S. Indris, S. L. Chou, Y. Huang, M. Wu and S. X. Dou, *Angew. Chem., Int. Ed.*, 2019, **58**, 1412–1416.

104 Y. Xiao, P.-F. Wang, Y.-X. Yin, Y.-F. Zhu, X. Yang, X.-D. Zhang, Y. Wang, X.-D. Guo, B.-H. Zhong and Y.-G. Guo, *Adv. Energy Mater.*, 2018, **8**, 1800492.

105 F. Zan, Y. Yao, S. V. Savilov, E. Suslova and H. Xia, *Funct. Mater. Lett.*, 2020, **13**, 2051016.

106 W. Shi, Y. Yan, C. Chi, X. Ma, D. Zhang, S. Xu, L. Chen, X. Wang and S. Liu, *J. Power Sources*, 2019, **427**, 129–137.

107 W. Zuo, J. Qiu, X. Liu, B. Zheng, Y. Zhao, J. Li, H. He, K. Zhou, Z. Xiao, Q. Li, G. F. Ortiz and Y. Yang, *Energy Storage Mater.*, 2020, **26**, 503–512.

108 M. Jia, H. Li, Y. Qiao, L. Wang, X. Cao, J. Cabana and H. Zhou, *ACS Appl. Mater. Interfaces*, 2020, **12**, 38249–38255.

109 L. Wang, J. Wang and P. Zuo, *Small Methods*, 2018, **2**, 1700293.

110 U. Maitra, R. A. House, J. W. Somerville, N. Tapia-Ruiz, J. G. Lozano, N. Guerrini, R. Hao, K. Luo, L. Jin, M. A. Perez-Osorio, F. Massel, D. M. Pickup, S. Ramos, X. Lu, D. E. McNally, A. V. Chadwick, F. Giustino, T. Schmitt, L. C. Duda, M. R. Roberts and P. G. Bruce, *Nat. Chem.*, 2018, **10**, 288–295.

111 Q. Li, S. Xu, S. Guo, K. Jiang, X. Li, M. Jia, P. Wang and H. Zhou, *Adv. Mater.*, 2020, **32**, 1907936.

112 K. Tang, Y. Huang, X. Xie, S. Cao, L. Liu, M. Liu, Y. Huang, B. Chang, Z. Luo and X. Wang, *Chem. Eng. J.*, 2020, **384**, 123234.

113 Y. You, A. Dolocan, W. Li and A. Manthiram, *Nano Lett.*, 2019, **19**, 182–188.